PAPER • OPEN ACCESS

Tungsten–carbon surface evolution and erosion modeling for a small angle slot divertor in DIII-D

OPEN ACCESS
IOP Publishing | International Atomic Energy Agency Nuclear Fusion
Nucl. Fusion **61** (2021) 126071 (10pp) https://doi.org/10.1088/1741-4326/ac36f4

Tungsten–carbon surface evolution and erosion modeling for a small angle slot divertor in DIII-D

J.N. Brooks[1,*], T. Sizyuk[2], G. Sinclair[3] and A. Hassanein[1]

[1] Purdue University, West Lafayette, IN, United States of America
[2] Argonne National Laboratory, Lemont, IL, United States of America
[3] General Atomics, San Diego, CA, United States of America

E-mail: brooks@purdue.edu

Received 17 August 2021, revised 26 October 2021
Accepted for publication 5 November 2021
Published 25 November 2021

Abstract

We modeled tungsten–carbon mixed surface evolution, sputtering erosion, and transport for the tungsten coated region of a small angle slot (SAS) divertor design for the DIII-D tokamak. This divertor concept aims to achieve a closed slot dissipative plasma to minimize heat load and surface erosion, and to study high-Z material performance. Our advanced simulations use coupled ITMC-DYN material mixing/response and 3D full kinetic REDEP/WBC erosion/redeposition code packages, with divertor plasma solution from the SOLPS-ITER package with 4 MW power input. The SAS design geometry and resulting in-slot plasma parameters cause significant differences in predicted sputter/transport from a conventional divertor. For 2% C/D incident plasma ratio, an equilibrium mixed C/W surface is attained at ∼30 s of discharge, from wall sputtered carbon transported to the 10 cm long tungsten divertor region. Tungsten remains exposed to the plasma, but the evolved surface composition varies with different C/D ratios. Tungsten is primarily sputtered from the mixed surface by impinging carbon ions in the +1 to +4 charge states, with some self-sputtering. Redeposition of sputtered tungsten to the divertor is significant, ∼80% along the higher plasma temperature attached plasma SAS entrance region, but this is less than the typically near-unity values for a conventional divertor. Plasma-incident carbon is highly backscattered (∼50%) from the mixed surface, with little redeposition (<10%); this helps maintain tungsten in the surface sputter zone. Carbon is mainly sputtered from the mixed surface by D^+ ions, also with low redeposition (∼10%–30%). Finally, the modeling shows non-zero but low sputtered tungsten current from the divertor to the core plasma direction. These results appear favorable for effective testing of a tungsten-containing SAS divertor in DIII-D, and extrapolation of mixed-material evolution/response findings to the analogous low-Z/high-Z, Be/W, ITER plasma facing system.

Keywords: tungsten divertor, C/W mixed surface material, DIII-D sputtering, small angle slot divertor

(Some figures may appear in colour only in the online journal)

* Author to whom any correspondence should be addressed.

1. Introduction

The small angle slot (SAS) divertor is a key element of divertor research on the DIII-D tokamak at General Atomics, e.g. [1–3]. The idea is to use a gas-tight slot geometry, together with recycling control through target shaping with glancing poloidal magnetic field angles, to achieve a dissipative plasma in the slot, with resulting moderate surface heat loads and low sputter erosion. Initial SAS experiments have been performed [4] as well as some plasma surface interaction modeling e.g. [2]. The DIII-D experiments showed that SAS enhances neutral cooling across the divertor target, with the divertor transitioning from the low recycling regime to the dissipative high recycling regime, at a relatively low density, an effect not usually achievable under typical H-mode conditions in DIII-D, as used in these SAS experiments [4]. Future SAS applications are envisioned for long pulse advanced tokamaks.

A new design called SAS-VW has been developed and is being constructed. This design modifies the original SAS shape to a V-shape baffle. This configuration change is predicted to improve detachment in the so-called favorable toroidal magnetic field direction [5, 6]. The new SAS-V configuration provides a strong concentrating effect of recycling deuterium neutrals toward the separatrix from both private and common flux sides of the outer divertor slot, further improving plasma cooling at the strike point relative to SAS [5].

The design includes a 10 cm long tungsten coated region at the outboard side of the V, in order to study high-Z material/plasma surface interaction, in support of future tokamak SAS applications. The rest of the divertor surface is bulk graphite, as is the DIII-D first wall. This paper describes our analysis of the expected tungsten region sputtering, transport, and surface evolution in SAS-VW, due to D^+ and carbon ion impingement from the edge plasma, and from sputtered/redeposited W and C ions.

Our purpose is to advance the understanding of material mixing and erosion/redeposition, aid the interpretation of DIII-D results, and assess application of this concept to future tokamak reactors. In this study we seek to identify general trends, with focus on three key questions: (1) will the tungsten surface remain exposed to the incident plasma ions (as opposed to being shielded by a carbon overlayer), thus enabling clearer data about plasma/tungsten interaction; (2) what are the expected gross and net W sputter erosion rates; and (3) in terms of potential core plasma impurity contamination, will the divertor-sputtered W flux to the edge plasma be acceptably small?

This work follows recent advanced plasma/surface simulations of several DIII-D removable divertor material evaluation system (DiMES) probe experiments [7]. The DiMES probe simulations used full-process, coupled material/response and full-kinetic, sub gyro-orbit, 3D erosion/redeposition code packages with near-surface input plasma parameters. These modeling tools are likewise employed for the present analysis. We have accounted for major differences, however, between DiMES and SAS. Namely, compared to DiMES (located in the more open DIII-D lower divertor), the SAS-VW tungsten divertor surface has a much shallower poloidal magnetic field angle (∼12–22° along the attached plasma region vs ∼65° for DiMES); is toroidally symmetric; has much lower entrance region plasma density (∼factor of 10); and—not being removable—will involve much longer exposure times. The latter point requires a complex, coupled analysis of the time-dependent mixed-material surface evolution, including carbon erosion/redeposition. Another difference is that the predicted SAS-VW near-surface peak electron temperature is higher, ∼40 eV vs 25 eV for the DiMES probe analysis. That raises a concern about high tungsten self-sputtering, although, to be discussed, this does not appear to be a problem for the cases examined here.

2. SAS-VW design

General features of the SAS concept are discussed in [1–3]. A recent paper further discusses the physics basis/goals behind the upgrade to SAS-VW [6]. These goals include exploiting the high collisionality enabled by a tightly baffled slot divertor geometry to suppress tungsten leakage in DIII-D, and using improved spectroscopy diagnostics with in-vacuo optics to measure the W gross erosion source from the divertor surface with high spatial and temporal resolution [6].

Figure 1 shows the DIII-D cross section and the SAS location, including the SOLPS-ITER computational grid. Figure 2 shows SAS-VW design cross section schematic details, in particular showing the 10 cm long tungsten coated outboard divertor segment; this is the experimental surface analyzed in this paper. The divertor is toroidally symmetric. The thickness of the W coating will be 10–15 μm. As stated, the other SAS-VW surfaces are graphite. Figure 2 also shows the larger divertor region, start of the scrapeoff layer (SOL) region, part of the core plasma, and the poloidal magnetic field lines and magnetic separatrix. This is for the case where the outer strike point is located at the vertex of the slot.

3. SOLPS-ITER modeling of edge/divertor plasma

3.1. Code methodology

The background plasma used to estimate the W region evolution and erosion was simulated via the SOLPS-ITER code package [8]. Both B2.5, a two-dimensional fluid plasma transport code, and EIRENE, a three-dimensional kinetic neutral transport code, are utilized to generate the plasma solution. The computational grid generated for the SAS-VW SOLPS-ITER modeling was based upon a previous DIII-D SAS discharge [4] (shot 176971 at time slice 3240 ms). This specific discharge had $B_t = -2$ T (ion $\boldsymbol{B} \times \nabla B$ drift out of divertor), $I_p = 1$ MA, and $P_{total} = 4.5$ MW. Modeling of the outer nose geometry of the SAS divertor was modified to enable the construction of a grid that smoothly extends out of the slot and onto the upper outer baffle, as done in [2]. The inner wall within the SAS divertor was also modified to mirror the geometry of the SAS-VW divertor (inner wall was moved closer to the outer wall, creating a V-shaped slot).

Input parameters used here for the SOLPS-ITER modeling are largely consistent with previous modeling of the DIII-D

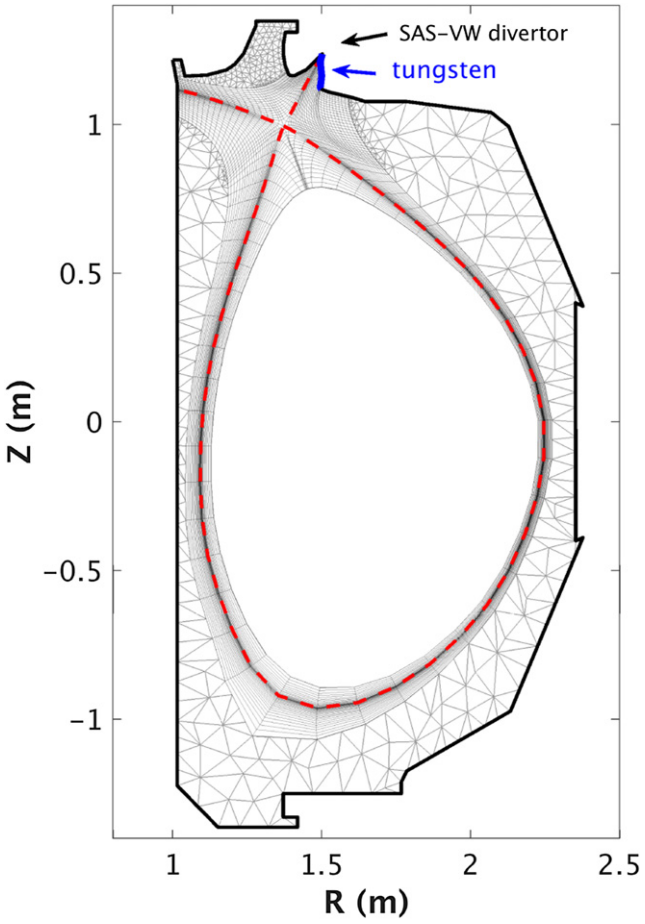

Figure 1. DIII-D tokamak cross section showing location of planned SAS-VW divertor, along with SOLPS-ITER grid for modeling plasma parameters. Blue line indicates region of tungsten coverage in slot.

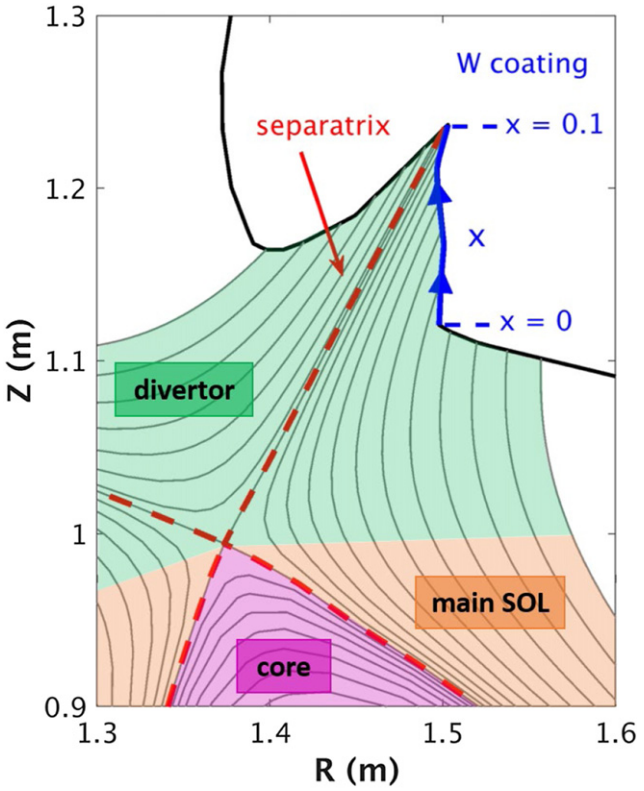

Figure 2. SAS-VW design geometry and surrounding regions. DIII-D tokamak major radius, R, and height parameter Z. Tungsten coating region analyzed here. 'x' coordinate measured from start of slot entrance region along the tungsten coated boundary. Strike point at $x = 0.1$ m.

tokamak [2, 9, 10] and have been tuned to optimize predictive capability. All charge states of C were simulated as were D^0 and D^+. One cryopump was simulated at the upper inner corner wall element, with a recycling fraction set to 70% (corresponding to 30% pumping fraction). Recycling was set to 100% on target surfaces and to 99% on the remaining wall surfaces. Physical sputtering of the graphite first wall was estimated using the Roth–Bohdansky model [11]. Chemical sputtering of the graphite wall was set at a constant 2% yield. The 4 MW of power crossing the separatrix (from a total power of 4.5 MW) was split evenly between electrons and ions. The leakage velocity in the private flux region (PFR) and common flux region (CFR) was set to 0.01% and 1% of the sound speed for the electrons and ions, respectively. The ion leakage flux was set at 1% and 0.1% of the ion sound speed flux in the CFR and PFR, respectively. Leakage parameters were chosen to be consistent with previous SOLPS-ITER modeling of SAS-VW [10]. The ion density at the innermost poloidal ring in the core region was set, based on previous DIII-D experimental Thomson scattering data, to 8×10^{19} m^{-3}, with plasma temperatures $T_e \sim T_i \sim 300$ eV. In the divertor region, the particle diffusivity was set to 0.3 m^2 s^{-1} and the ion/electron thermal diffusivity was set to 1 m^2 s^{-1}, consistent with earlier SOLPS-ITER modeling on DIII-D [2]. However, the transport coefficients used in the SOL region were based on experimental Thomson scattering data via an iterative coupling process detailed in [12]. The SOLPS-ITER simulations shown do not include the effect of particle drifts.

3.2. SOLPS-ITER plasma background

The resulting plasma solution in the volume along and near the W coated region, obtained using SOLPS-ITER, is used as an input into the coupled REDEP/WBC and ITMC-DYN code packages, to analyze the W coating surface performance in SAS-VW. Radial profiles of T_e and T_i across the W target region, at the sheath boundary, are shown in figure 3. The corresponding plasma electron density profile is shown in figure 4. Per figure 2 the '$x = 0$' notation refers to the position near the SAS-VW slot entrance where the tungsten coating starts. The plasma is seen to be roughly divided into a 7 cm attached region and a 3 cm detached region. We characterize the detached region, for the present purposes, as occurring

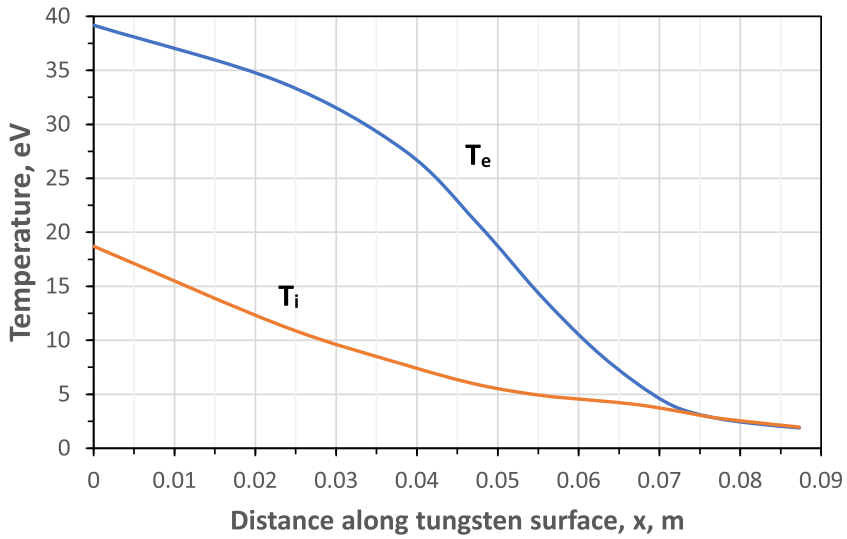

Figure 3. Plasma electron and ion temperature profile along the tungsten portion of the DIII-D SAS-VW divertor design. Values at sheath boundary. From SOLPS-ITER plasma code solution. Attached plasma obtains from about $0 \leqslant x < .07$ m; detached plasma for $x \geqslant .07$ m.

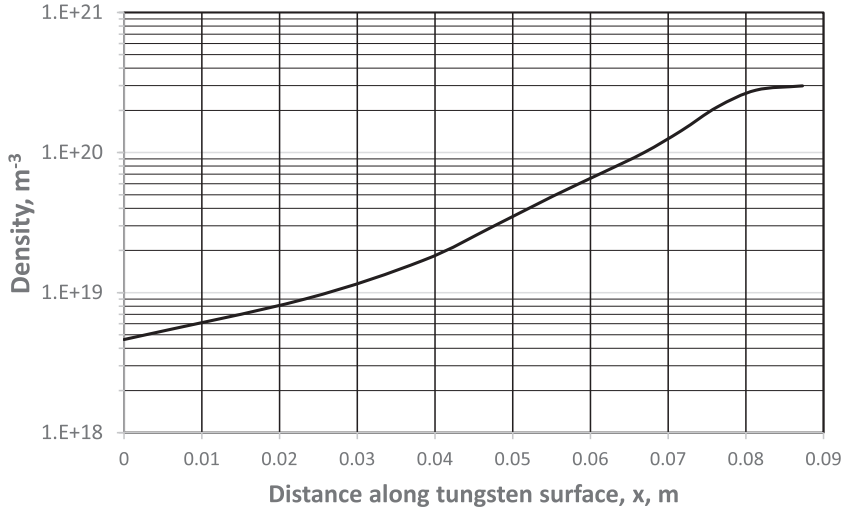

Figure 4. Plasma electron density profile along the tungsten portion of the DIII-D SAS-VW divertor design. At sheath boundary. From SOLPS-ITER plasma code solution.

where T_e and T_i are both lower than 5 eV. For those conditions sputter yields and rate coefficients for sputtered impurity atom electron impact ionization decrease substantially. At and near the slot vertex ($x = 0.1$ m), high plasma densities, as well as high neutral recycling fluxes, cool the plasma, with T_e and T_i falling well below 10 eV. Outboard from the slot vertex (decreasing x) the plasma temperature increases as the cooling effect of the slot diminishes, corresponding to an attached divertor condition. The opening in the slot, referred to as the progressive angle, reduces the rate of increase in plasma temperature, as described in the original SAS design paper [1]. At the slot entrance T_e reaches a maximum of ~40 eV. From the slot vertex to the slot entrance, electron density drops by almost two orders of magnitude, demonstrating the strong effect of the closed slot geometry on local particle confinement. Work in [2, 6, 10] provides a more detailed assessment of the SAS-VW geometry and how it impacts the divertor plasma.

4. Surface evolution and erosion

4.1. Mixed C/W surface formation

Given the geometry, magnetic field, and SOLPS-ITER plasma solution, we use the ion transport in materials and compounds-dynamics (ITMC-DYN) and REDEP/WBC code packages to compute the SAS-VW surface evolution and sputter erosion/redeposition along the initially pure-tungsten coated region shown in figure 2. The ITMC package is described in e.g. [13, 14]. This package integrates all collisional and near surface thermal processes to study the effect of impurities, surface segregation, hydrogen isotope retention, and erosion

in plasma facing materials under multiple mixed ions irradiation during steady state and transient events. ITMC simulations have been benchmarked against laboratory experiments as well as NSTX experiments [15].

The REDEP/WBC code package, e.g. [16, 17], is a 3D, full-kinetic, Monte Carlo, sub-gyro-orbit, erosion/redeposition simulation tool. This package has also been benchmarked, e.g. against various tokamaks [7, 17]. REDEP/WBC, to our knowledge, includes all relevant impurity sputtering and transport processes, including Lorentz force motion, plasma/impurity collisions, oblique magnetic field incidence sheath structure, atomic and molecular processes, and diffusion.

SOLPS inputs to WBC for this analysis are the near-surface plasma 2D spatial profiles (N_e, T_e, T_i, flow velocity, pre-sheath electric field, etc), and impinging deuterium and carbon atom/ion particle fluxes. WBC then computes the incident particle angles and energies, accounting for pre-sheath and sheath-acquired energies. WBC then launches individual W and C atoms from the divertor surface, via Monte Carlo, using ITMC computed sputtered and backscattered yields, and energy and angular probability distributions. The emitted atoms are subject to electron impact ionization and atom/plasma elastic collisions. Resulting ions are tracked in 3D via Lorentz force motion and plasma/impurity collisions. A sputtered particle history terminates upon redeposition to the surface or leaving the tungsten SAS-VW region. Redeposited particles can stick to the surface, sputter carbon and/or tungsten, or backscatter. Backscattering is high for carbon, to be discussed, and low for tungsten. Sputtered and backscattered atoms are launched as new particle histories and their transport likewise followed. A typical WBC computation, at any spatial segment, and any fixed time, involves $\sim 10^5$ histories.

Since DIII-D is a carbon surface tokamak, an obvious important parameter for any DIII-D plasma/surface interaction analysis is the carbon concentration in the impinging plasma. Based on past studies, available DIII-D data, e.g. as discussed in [7], and present (but somewhat uncertain) SOLPS results, we have adopted a reference value of 2% C/D for this study. To assess sensitivity, we ran simulations for surface evolution using plausible alternative concentration values of 1% and 3%.

Our analysis uses an iterative coupling procedure between WBC for sputtered tungsten and carbon transport and redeposition, and ITMC computation of surface elemental composition and tungsten and carbon sputter yields and sputtered atom velocities. The iteration starts with the initially pure-W surface and ends at the surface equilibrium time. A complete coupling, at each spatial point and time step, would be computationally challenging, and is not needed for the present purposes of identifying key trends. We instead use a selected, limited, number of space/time iterations, with focus on the attached plasma region. Numerical testing/sampling has shown that our conclusions are reasonably insensitive to this limit, again for the present purposes.

Figure 5 shows the computed tungsten and carbon depth profiles, at a typical point near the start of the attached plasma

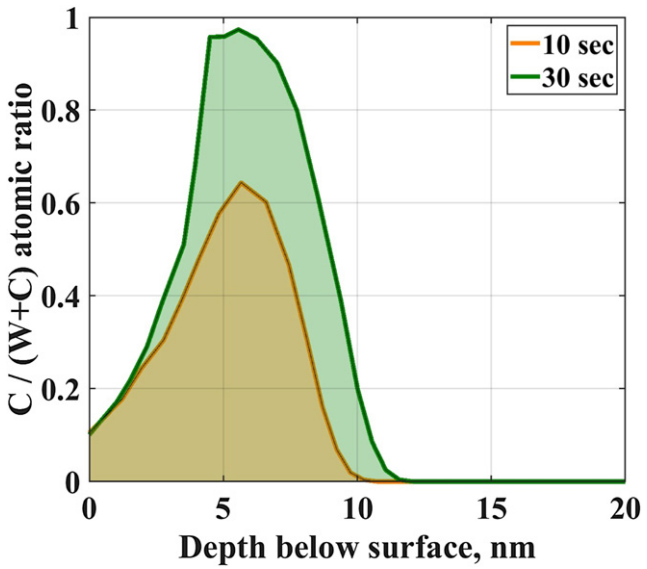

Figure 5. Time-dependent tungsten–carbon surface composition depth profile, at attached plasma point $x = .02$ m in the DIII-D tokamak SAS-VW divertor W region. For impinging carbon plasma concentration, C/D, of 2%. ITMC code package calculation with coupled WBC/SOLPS inputs of D, C, W ion species impingement and redeposition fluxes/energies. Equilibrium reached at about 30 s.

divertor region, at times 10 and 30 s. The surface evolution is qualitatively similar along the attached plasma region. The position of the 'surface' (depth '0' in figure 5) is actually growing with time with respect to the divertor initial surface position. This expansion is due to C implantation and the difference in densities of W and C. There is already a substantial amount of carbon embedded in the surface at 10 s. Equilibrium is reached at about 30 s (notwithstanding migration of W from the bulk surface due to a small net loss, of order 0.1 nm s^{-1}). At equilibrium, tungsten remains dominant at the very near surface, ~0–3 nm, with carbon dominating until about 8 nm depth, with the carbon concentration then dropping off sharply.

It is important to note that sputtering occurs from various depths in the surface, depending on the particle type and incident energy/angle. For carbon ions along the attached region, incident energies range from about 200–500 eV, with incident elevation angles averaging about 45°. For example, at the divertor entrance, with peak $T_e \sim 40$ eV, a C^{+3} ion—this species comprising about 30% of the carbon ion flux—is accelerated through the $3kT_e \sim 120$ V sheath potential, and impinges with ~500 eV energy, also considering its average pre-sheath energy. (There is also some higher energy carbon flux, in particular C^{+4} at ~615 eV, but comprising only about 5% of the total.) Tungsten sputtering is found from ITMC to occur from a depth of about three monolayers, corresponding to about 1 nm in the mixed material.

The key finding is that the equilibrium surface retains more than enough tungsten to permit plasma/surface interaction with the tungsten, thus enabling high-Z plasma/surface interaction experiments.

4.2. Erosion/redeposition

Per this modeling, tungsten in the SAS surface is mostly sputtered by carbon ions in the +1 through +4 charge states, with some self-sputtering, and small contributions from C^0 and C^{+5}. Impinging D^+ energies are below the W sputtering threshold. In contrast, deposited carbon in the surface is primarily sputtered by D^+, with some sputtering from W and C. As expected, there is no W sputtering in the detached plasma surface region ($x \geqslant 7$ cm).

An important finding in our simulations concerns backscattered carbon. For a single-element plasma facing surface, of any material, and for typical divertor plasma conditions, backscattering of incident surface material ions is a minor process. However, for the low *Z*/high *Z* mixed surface ITMC predicts a high impinging C backscatter fraction, e.g. 46% for the first 2 cm of the attached plasma region. The high C backscatter is due to binary collision, ballistic scattering, of the low mass carbon atoms off high mass tungsten atoms. WBC simulations of the backscattered carbon atom transport, using ITMC launch statistics (at average energy ∼3× higher than sputtered carbon), show little redeposition (<10%) to the W surface. Instead, almost all backscattered C will deposit elsewhere in the slot divertor (we do not track this deposition since we are concerned here only with the W surface region response). The high backscatter of carbon from the mixed surface is thus an important factor for maintaining a tungsten presence in the mixed C/W surface, by minimizing the retained carbon. This seems to be a unique and important characteristic of a low-*Z*/high-*Z* mixed material fusion surface.

Table 1 summarizes tungsten and carbon sputtering erosion/redeposition parameters for the first part of the W segment in the attached plasma region. The redeposition parameters for tungsten do not vary greatly along the attached plasma region. Sputtered carbon redeposition fractions increase along the region (increasing *x*) but are low in any event. Sputtered particle transport depends first on the ionization mean free path for sputtered atoms, and subsequent, complex, ion transport processes. The sputtered carbon atom mean free path is much greater (∼×4) than for tungsten. This difference is due to the lower carbon mass, higher sputtered velocity (for similar launch energy), and smaller carbon electron impact ionization cross sections. Once ionized, impurity transport depends, among other things, on the poloidal magnetic field geometry. The poloidal field angles for the SAS-VW tungsten region vary from about 12–22° from tangential, thus more oblique than the ∼65° for typical DiMES probe and open lower DIII-D divertor geometry. This, by itself, reduces local redeposition. Also, as mentioned in the SOLPS results description, the initial electron density is low. The table 1 listed tungsten redeposition, at 80%, is high. However, this is significantly less than the near 100% redeposition predicted for a non-slotted divertor, e.g. JET [18] or ITER [19]. Likewise, DiMES probe simulations show complete W redeposition on either the probe itself or the rest of the bottom divertor [7]. The lower SAS-VW redeposition fraction has some consequences, to be discussed, for net sputter erosion rates and loss of sputtered material from the SAS-VW divertor W surface.

Tungsten redeposition fractions are similar along the slot, in the attached plasma region going toward the strike point. This is due to the lower electron temperatures/lower ionization rate coefficients tending to offset the higher electron densities. In general, W and C ion local redeposition physics is dominated by collisional friction with the incoming plasma and Lorentz force motion. (Images of typical sputtered W trajectories can be seen in figure 1 of reference [7] for DiMES simulations; the general features of W atom ionization, W ion ionization into higher charge states, gyromotion, and redeposition are qualitatively similar for the SAS divertor.)

The redeposition fraction of the sputtered carbon varies from ∼12%–30% along the attached plasma region. This low carbon redeposition also contributes to maintaining tungsten in the mixed surface.

An encouraging result is that the WBC-ITMC predicted average W self-sputter yield (peak of ∼0.25) is much lower than the ∼1.0 or higher value that could cause self-sputtering runaway. This is due to average W ion redeposition transit times being short enough to limit ionization into high charge states and corresponding high sheath-acquired energy. The mean W ion redeposition energy (even with high variance) along the W surface is well below the ∼700–1000 eV range needed for unity or greater sputter yields, for the computed near-normal elevation angle incidences.

Figure 6 shows gross and net sputter-eroded tungsten flux spatial profiles. We observe gross erosion peaking in the attached plasma region and falling to zero in the detached region. Net erosion is substantially lower than gross erosion, and also involves a region of small W *growth*; this due to transport of non-locally redeposited sputtered material along the '*x*' axis. The peak net tungsten erosion flux of 5.9×10^{18} m^{-2} s^{-1} is equivalent to a loss of ∼0.1 nm s^{-1}. This is insignificant for DIII-D SAS-VW experiments, in terms of maintaining a tungsten coating throughout the entire experimental campaign.

In terms of potential core plasma high-*Z* contamination, the total W sputtered current is 2.68×10^{19} s^{-1}. The W current leaving the slot toward the core plasma ($x < 0$) is 5.44×10^{17} s^{-1}, or only 2% of the sputtered total. This latter current all comes from the first ∼2 cm of the divertor. The SAS-VW geometry helps in this regard. The W current to the *core plasma* would be expected to be highly attenuated from the above value due to transport processes in the entire divertor region, whereby the W ions are entrained in the outgoing plasma and returned to the slot or other material boundaries. Low core plasma W contamination was seen experimentally for full toroidal tungsten rings in DIII-D, e.g. [20], although for a different divertor system and boundary conditions. For the SAS-VW divertor, this needs detailed study such as by REDEP/WBC tungsten ion transport analysis for the entire divertor region, coupled to edge/core plasma transport codes, also examining the effect of particle drifts on the plasma background.

5. Other cases

We ran simulations for two additional plasma incident C/D ratios, as mentioned to assess sensitivity to this parameter.

Table 1. Summary of tungsten and carbon sputtering erosion/redeposition parameters for a DIII-D tokamak SAS divertor design. WBC/ITMC coupled code package analysis; plasma parameters from SOLPS-ITER code. For attached plasma SAS-VW divertor segment, $0 < x < 2.32$ cm, toroidally continuous; mixed C/W surface at equilibrium.

Parameter	Tungsten	Carbon
Pre-sheath plasma temperatures and density (at slot entrance)	$T_e = 39$ eV, $T_i = 19$ eV, $N_e = 4.6 \times 10^{18}$ m^{-3}	
Mean sputtered atom energy	24 eV	38 eV
Mean-free-path for sputtered atom ionization (normal to surface)	1.8 mm	8.7 mm
Transit time (ionization to redeposition)[a]	3.4 (6.9) μs	8.0 (12) μs
Charge state[a]	2.0 (1.4)	1.4 (.59)
Energy[a]	244 (250) eV	193 (94) eV
Elevation angle of incidence[a] (from normal)	19 (11)°	43 (13)°
Self-sputtering coefficient[a]	.24	.11
Redeposition fraction	.80[c]	.12
Sputtered tungsten transport fraction to plasma	.083[d]	—
Gross sputtered tungsten flux[b], 10^{19} m^{-2} s^{-1}	3.70	—
Net sputtered tungsten flux[b], 10^{19} m^{-2} s^{-1}	0.49	—

[a]Average, and where shown (standard deviation), for redeposited ions on indicated segment.
[b]Average over segment.
[c]Includes ∼10% transport contribution from rest of divertor.
[d]From the segment; W transport to plasma is negligible from rest of divertor.

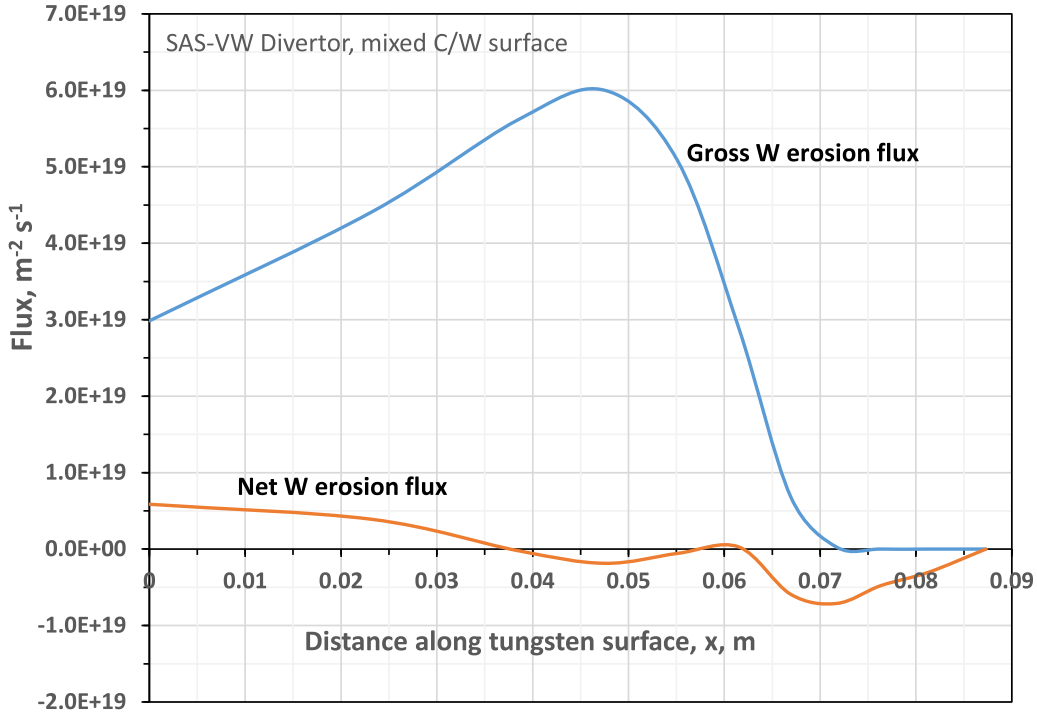

Figure 6. Gross and net sputter-eroded tungsten flux along the DIII-D tokamak SAS-VW divertor design. REDEP/ITMC coupled code package simulation, SOLPS-ITER plasma solution. For C/W mixed surface structure and sputter yields/velocities at equilibrium (30 s). Note region of net deposition in and around detached plasma region.

These simulations focused on ITMC computation of surface evolution, using the same WBC-computed particle/energy inputs as the 2% case, thus not fully self-consistent but we believe appropriate to show trends. Figures 7 and 8 show results for C/D 3% and 1% cases, respectively. The higher carbon content 3% case, not surprisingly, shows more C coverage in the mixed-material surface than the reference case, although still with high W surface concentration. In fact, since the surface composition is similar in the first several monolayers, the W sputter yields are very similar to the 1% case. The carbon yields, however, are higher, as is sputtered C transport to the detached plasma region.

The 1% case, again as expected, shows less but still significant C coverage. The W sputter yields are also about the same as for the reference case, but with lower C yields.

Future work is needed to make quantitative predictions, but the initial conclusion is that we would expect similar looking net tungsten erosion profiles over this broad range of C/D ratios, thus enabling the study of high-Z sputtering, transport, and redeposition in DIII-D SAS-VW experiments.

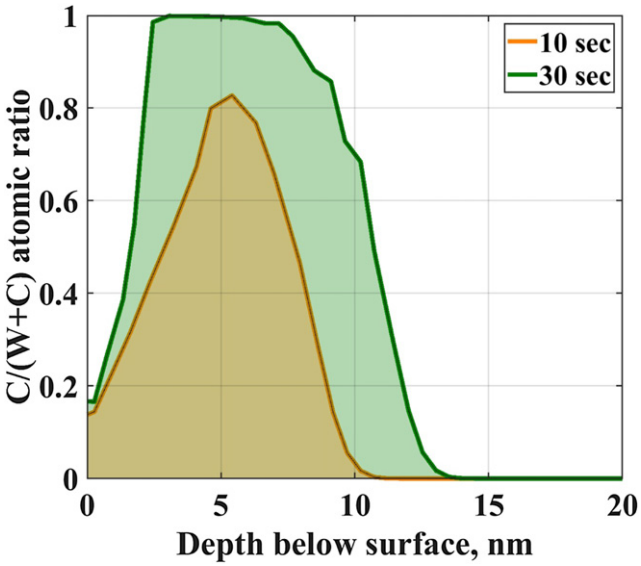

Figure 7. Time-dependent tungsten–carbon surface composition depth profile; same point and conditions as figure 5, but plasma carbon concentration of 3%. ITMC/WBC calculation.

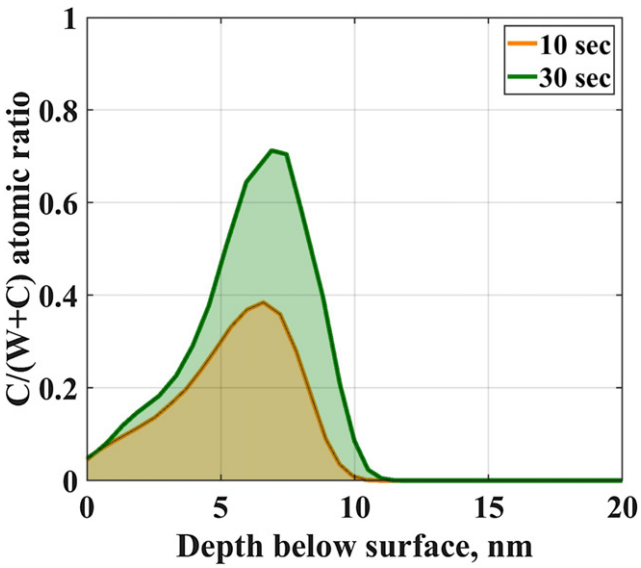

Figure 8. Time-dependent tungsten–carbon surface composition depth profile; same point and conditions as figure 5, but plasma carbon concentration of 1%. ITMC/WBC calculation.

We assessed the sensitivity of the redeposition rates and sputtered W current fraction to the plasma to some variations (∼25%) of the attached region near-surface plasma temperatures and density (lower T_e, T_i, higher N_e). Although the absolute tungsten fluxes/currents obviously change, the qualitative trends remain the same.

6. Discussion

The addition of particle drifts ($\boldsymbol{E} \times \boldsymbol{B}$, $\boldsymbol{B} \times \nabla B$, and viscosity) to the plasma background can impact the extent of the attached plasma region and alter quantitative estimates of both the sputtered gross/net W flux and the W current leaving the slot. However, per the present analysis, the key qualitative dependence of these fluxes and currents on the SAS shallow poloidal angle geometry and slot entrance region low-density/high-temperature plasma characteristics would be the same. In any event, future work using ITMC-DYN and REDEP/WBC can incorporate these plasma backgrounds with particle drifts to improve the predictive capability of time-dependent surface evolution and erosion estimates in SAS-VW.

Regarding extrapolation of the SAS-VW surface evolution and erosion results to ITER, the ITER beryllium first wall and tungsten vertical divertor combination is reasonably analogous to the DIII-D C/W system, in terms of low-*Z*/high-*Z* material mixing, physical sputtering erosion, and hydrogen isotope trapping. The modeling techniques here for DIII-D, and the expected SAS-VW experimental data, can therefore be useful to assess the formation of a stable Be/W ITER divertor surface and erosion response. We note that divertor power loading will be higher in ITER, but this would be partially offset by lower Be on W sputter yields compared with C on W.

The SAS-VW mixed C/W surface in DIII-D will retain impinging and diffusing deuterium via D trapping in carbon. The D trapping rate depends on the surface carbon concentration and depth profile, such as shown in figure 5 for the reference C/D ratio. Deuterium retention is an important study area in DIII-D but is not directly critical to the SAS performance, and we did not focus on D trapping analysis in our present work. However, tritium trapping and inventory in ITER mixed/co-deposited Be/W surfaces is of major importance. DIII-D SAS experiments and modeling can thus be used to help estimate ITER D–T retention/recycling and tritium inventory. Further analysis by us is possible, to examine C/W and Be/W mixed-material co-deposited D and T trapping in detail, building on the present results.

7. Conclusions

This work uses coupled plasma edge/SOL, dynamic surface mixing, and erosion/redeposition code packages, to model the surface evolution and sputter response of the planned SAS-VW, SAS divertor with a tungsten surface, in the DIII-D tokamak. The predicted divertor plasma along the toroidally continuous, 10 cm long W surface, has two basic elements; a low density/high temperature (∼40 eV peak) attached plasma entrance region, and a high density/low temperature (<5 eV) detached region at/near the strike point. This plasma structure and SAS divertor magnetic and spatial geometry determine the basic trends found. These trends and general conclusions are reasonably insensitive to several key parameters, including the plasma carbon content from wall sputtering, and moderate changes in plasma temperatures and density along the tungsten boundary.

For the computed D, C, and W ion fluxes in question, the initially pure W, attached plasma region divertor surface evolves into a mixed C/W surface, of depth 12 nm, and reaches equilibrium in ∼30 s. The mixed material surface has

a complex structure with substantial carbon fraction. Tungsten remains dominant in the critical ∼0–3 nm surface zone, and is sputtered by plasma impinging C, and redepositing C and W ions. The non-zero W sputtering will permit experimental testing of sputtered and transported tungsten for DIII-D SAS-VW experiments. Carbon is also sputtered from the mixed material, primarily by D ions, with C generally redepositing deeper into the slot.

The peak W sputter erosion rate, of order 0.1 nm s^{-1}, is inconsequential for DIII-D operations. Modeling, however, shows a low but non-trivial W current leaving the slot divertor region and going in the core plasma direction. This loss current arises from a ∼2 cm long segment of the W surface at the start of the attached plasma region. The W loss current is not likely to be a concern to core plasma quality, but this needs detailed edge/core plasma impurity transport analysis and experimental validation.

Our future plans include refining details of the present results, examining design and plasma variations for DIII-D, including the addition of particle drifts to the plasma background; investigating slot-escaping W transport in the full divertor region; and examining relevant issues for various fusion tokamaks, including trapping and retention estimates for hydrogen isotopes in co-deposited mixed C/W and Be/W systems.

Disclaimer

Acknowledgments

Work supported by the US Department of Energy, Office of Science/Office of Fusion Energy Sciences, under Purdue University Award DE-SC0020198; and in part using the DIII-D National Fusion Facility, a DOE Office of Science user facility, under Award DE-FC02-04ER54698.

ORCID iDs

T. Sizyuk https://orcid.org/0000-0003-0851-8632
G. Sinclair https://orcid.org/0000-0003-4195-177X

References

[1] Guo H.Y., Sang C.F., Stangeby P.C., Lao L.L., Taylor T.S. and Thomas D.M. 2017 Small angle slot divertor concept for long pulse advanced tokamaks *Nucl. Fusion* **57** 044001
[2] Ma X., Abrams T., Covele B., Elder J.D., Guo H.Y., Guterl J. and Stangeby P.C. 2020 Evaluation of the impact of divertor closure on high-*Z* material transport and leakage in small angle slot divertor with toroidal tungsten rings in DIII-D *Phys. Scr.* **T171** 014072
[3] Casali L., Covele B.M. and Guo H.Y. 2019 The effect of neutrals in the new SAS divertor at DIII-D as modelled by SOLPS *Nucl. Mater. Energy* **19** 537
[4] Guo H.Y. *et al* 2019 First experimental tests of a new small angle slot divertor on DIII-D *Nucl. Fusion* **59** 086054
[5] Du H., Guo H.Y., Stangeby P.C., Bonnin X., Zheng G., Duan X. and Xu M. 2020 Manipulation of $E \times B$ drifts in a slot divertor with advanced shaping to optimize detachment *Nucl. Fusion* **60** 126030
[6] Abrams T. *et al* Design and physics basis for the upcoming DIII-D SAS-VW campaign to quantify tungsten leakage and transport in a new slot divertor geometry Phys. Scr. (submitted).
[7] Brooks J.N., Sizyuk T., Elder J.D., Abrams T., Hassanein A., Rudakov D.L. and Wampler W. 2020 Modeling, analysis, and code/data validation of DIII-D tokamak divertor experiments on ELM and non-ELM plasma tungsten sputtering erosion *Nucl. Fusion* **60** 126026
[8] Wiesen S. *et al* 2015 The new SOLPS-ITER code package *J. Nucl. Mater.* **463** 480
[9] Ma X., Wang H.Q., Guo H.Y., Stangeby P.C., Meier E.T., Shafer M.W. and Thomas D.M. 2021 First evidence of dominant influence of $E \times B$ drifts on plasma cooling in an advanced slot divertor for tokamak power exhaust *Nucl. Fusion* **61** 054002
[10] Maurizio R. *et al* 2021 Numerical assessment of the new V-shape small-angle slot divertor on DIII-D *Nucl. Fusion* **61** 116042
[11] Roth J. and Garcia-Rosales C. 1996 Impurity generation processes in particle-surface interaction: data status and needs *Atomic and Plasma-Material Interaction Processes in Controlled Thermonuclear Fusion* vol 36 p 1647
[12] Canik J.M., Maingi R., Soukhanovskii V.A., Bell R.E., Kugel H.W., Leblanc B.P. and Osborne T.H. 2011 Measurements and 2D modeling of recycling and edge transport in discharges with lithium-coated PFCs in NSTX *J. Nucl. Mater.* **415** S409
[13] Hassanein A. 1985 Surface effects on sputtered atoms and their angular and energy dependence *Fusion Technol.* **8** 1735
[14] Sizyuk T. and Hassanein A. 2010 Dynamic analysis and evolution of mixed materials bombarded with multiple ions beams *J. Nucl. Mater.* **404** 60
[15] Sizyuk T. and Hassanein A. 2013 Dynamic evolution of plasma facing surfaces in NSTX: impact of impurities and substrate structure on fuel recycling *J. Nucl. Mater.* **438** S1109
[16] Brooks J.N. 1990 Near-surface sputtered particle transport for an oblique incidence magnetic field plasma *Phys. Fluids* **8** 1858
[17] Brooks J.N. 2002 Modeling of sputtering erosion/redeposition—status and implications for fusion design *Fusion Eng. Des.* **60** 515
[18] Kirschner A. *et al* 2019 Modelling of tungsten erosion and deposition in the divertor of JET-ILW in comparison to experimental findings *Nucl. Mater. Energy* **18** 239
[19] Brooks J.N., Allain J.P., Doerner R.P., Hassanein A., Nygren R., Rognlien T.D. and Whyte D.G. 2009 Plasma–surface interactions of an all-metal ITER *Nucl. Fusion* **49** 035007

[20] Wampler W.R., Rudakov D.L., Watkins J.G., McLean A.G., Unterberg E.A. and Stangeby P.C. 2017 Measurements of tungsten migration in the DIII-D divertor *Phys. Scr.* **T170** 014041